

Strain mediated Adatom Morphologies on Cu<111>, a Monte-Carlo Simulation.

W.Kappus

v01: 2012-07-27

Abstract

Substrate strain mediated adatom configurations on Cu<111> surfaces have been Monte Carlo simulated in a coverage range up to nearly 1 monolayer. Interacting adatoms occupy positions on a triangular lattice in two dimensions. The elastic interaction is taken from earlier calculations, short range effects are added for comparison. Dependent on the coverage different morphologies are observed: Superlattices of single adatoms in the 0.04 ML region, ordered adatom clusters in the region of 0.1 to 0.3 ML, elongated islands in the 0.4 ML region and interwoven stripes in the 0.5 ML region. In the region above the sequence is reversed with occupied and empty positions complemented. Stronger short range interactions increase the feature size of the clusters and reduce their lattice order. The influence of the substrate elastic anisotropy turns out to be significant. Though quite different in dimension, sample results are compared with strain relief observations on Cu<111> surfaces.

1.Introduction

Regular self-assembled adatom structures, ranging from superlattices via nanodot arrays to strain relief stripes are interesting for various general and technological reasons, reviews were given in [1,2]. Calculations of the stability and dynamics of strain mediated superlattices in a low coverage region [3] left the question open how adatoms arrange under equilibrium conditions when the coverage is increased. The beautiful experiments of Plass et al. on domain patterns [4] provides insight in this topic and a challenge to prove the ability of an elastic continuum theory to build a bridge between superlattices and stress relief patterns.

In this work, based on [3,5,6,7], Monte Carlo simulations of elastic adatom interactions on Cu<111> are adapted to coverages up to nearly 1 monolayer. The simulation is restricted to two-dimensional adatom configurations on identical sites of the surface. In section 2 the model details are recalled and slightly modified against [3]. In section 3 the results of Monte Carlo simulations are

presented. In section 4 consequences of increasing coverages and of alternative short range interactions are discussed. Also open questions are addressed. Section 5 closes with a summary of the results.

2. Model Details

2.2. Elastic Interactions of Adatoms

Following [7] the interaction of adatoms located at the origin and s using polar coordinates (s, ϕ) for their distance $s = |\vec{s}|$ and pair direction angle ϕ with respect to the crystal axes is given by

$$U(s, \phi) = (2\pi)^{-1} \sum_p \omega_p \frac{\cos(p\phi) \cos(p\frac{\pi}{2}) \Gamma(\frac{p+3}{2}) s^p {}_1F_1\left(\frac{p+3}{2}; p+1; \frac{-s^2}{4\alpha^2}\right)}{2^{p+1} \Gamma(p+1) \alpha^{p+3}}, \quad (2.1)$$

where ${}_1F_1$ denotes the Hypergeometric Function, $\Gamma(p)$ the Gamma function, $\alpha = \sqrt{2}/2$ is a cutoff length defining height and location of the potential wall and the medium range potential, and the ω_p denote coefficients of a cosine series describing the solution of an elastic eigenvalue problem [7]. The dominating isotropic $p=0$ term of (2.3) is negative for small s describing a potential well (i.e. an attractive potential), has a positive wall (i.e. a repulsive potential) at $s=s_w$ and approaches infinity with a s^{-3} law. For elastic anisotropic substrates like Cu the $p>0$ terms describe the anisotropic part of the interaction and influence the height of the positive wall in dependence of the pair direction angle ϕ with respect to the crystal axes. Tab. 1 shows the ω_p for the elastic adatom interaction on Cu<111> and W<111> (for comparison) calculated as outlined in [7]. We note the units of the ω_p :

- the numerator is P^2 , the square of a scalar parameter P describing the lateral stress magnitude an adatom exerts to the surface
- the denominator is the c_{44} elastic constant of the substrate.

For details of the parameter P see [7].

Substrate	c_{11}	c_{12}	c_{44}	ζ	ω_0	ω_6	ω_{12}
Cu	169.	122.	75.3	-1.376	-1.01	-0.007	+0.0004
W	523.	203.	160.	0.	-0.720	0.	0.

Table 1. Substrate Elastic Constants c_{ik} (GPa) from [8], anisotropy $\zeta = (c_{11} - c_{12} - 2c_{44})/c_{44}$ and coefficients ω_p (in P^2/c_{44} units) on Cu <111> and W<111>

In the present analysis the strong attractive interaction of (2.1) in the region $s < s_w$ is replaced by three variants to study the influence of short range interactions - in addition to the elastic interaction - on the medium range adatom

morphology:

- variant 1 as used and described in [3]

$$U_1(s, \phi) = U_w + U_{wp} \cos(p\phi) \frac{s}{s_w} \text{ for } s < s_w, \quad (2.2)$$

where U_w describes the wall height, U_{wp} the wall anisotropy variance, and s_w is the location of the wall maximum,

- variant 2, describing additional attraction between next neighbors

$$U_2(s, \phi) = 0 \text{ for } s < s_0, \quad (2.3)$$

where s_0 is defined by $U(s_0, \phi) = 0$, covering the range $s \lesssim 1.75$, significantly smaller than s_w ,

- variant 3, describing stronger attraction between next neighbors

$$U_3(s, \phi) = -5 k_B T \text{ for } s \leq s_3, \quad (2.4)$$

where s_3 is the next neighbor distance. The value -5 is chosen to get an equidistant series of U values.

2.3. Monte-Carlo Simulations

The grid-less algorithm used in [3] turned out unstable and inefficient in the coverage range $\theta > 0.1$. Therefore a triangular grid algorithm has been used instead. The triangular grid represents adatom positions on a $\langle 111 \rangle$ surface with threefold symmetry fulfilling the symmetry condition used for the adatom generated surface stress [7]. Periodic boundary conditions were applied to avoid the problem of adatom diffusion to the boundary. The hexagon diameter of 48 units was chosen to keep the computing time in the range of hours while the interaction $u(s=24)$ has decreased well below 0.01. Temperature effects are treated by the normalized interaction

$$u(s, \phi) = U(s, \phi) / k_B T. \quad (2.5)$$

Not knowing the size of the stress parameter P and as in [3] the average wall height is assumed $u_W=5$ and this choice determines all $u(s, \phi)$.

In our grid algorithm an adatom configuration is described by a set of occupation numbers $\{\tau_i\}$, $\tau_i \in \{0, 1\}$. Starting from a random k member adatom configuration $\{\tau_{i,0}\}$, step $n+1$ $\{\tau_{i,n+1}\}$ evolves from step n $\{\tau_{i,n}\}$ by comparing the total interaction of each adatom i

$$u_{\text{tot}}(i) = \sum_{j=1}^k u_{ij} \tau_j \quad (2.6)$$

with that of its empty next neighbor positions. If a next neighbor position m has less total interaction, the adatom i jumps to that position m. So adatoms move around under the force field of all neighbors until all interaction is minimized.

The iterations are terminated when either no more jumps occur or when loops of identical configurations are detected.

2.3. Pair Distribution

The adatom pair distribution g_{ik} is calculated by averaging occupation pairs

$$g_{ik} = \langle \tau_i \tau_k \rangle / \theta^2, \quad (2.6)$$

where θ denotes the coverage. So $g_{ik}=1$ in a random configuration, $g_{ik}>1$ if the pair $\{\tau_i, \tau_k\}$ occurs more likely and $g_{ik}<1$ if the pair $\{\tau_i, \tau_k\}$ occurs less likely. It is the discrete variant of $g(s, \theta)$ calculated in [5] with a 2-dimensional Born-Green-Ivon type integral equation.

2.4. Pair Distribution Scaling

For the discussion of experimental results in section 4.5 we will need to recall scaling properties of the continuous pair distribution $g(s, \theta)$ as outlined in [5]. In the long range isotropic limit the adatom-adatom interaction becomes

$$u_3(s) = u_0 s^{-3} \quad (2.7)$$

and the pair distribution scales

$$g(s, u_0, \theta) = g(\tau s, \tau^3 u_0, \tau^{-2/3} \theta) \quad (2.8)$$

with a scaling factor τ . In other words the pair distribution has the same shape if simultaneously the length is doubled, the interaction is eightfold and the coverage is reduced by a factor of about 0.63. We also note from eq. (2.5) an eightfold normalized interaction u results if the interaction U is kept constant and the temperature T is reduced by a factor eight. We further note that doubling the stress parameter P increases the interaction U by a factor 4.

3. Results

3.1. Reference Configuration

The presentations show empty and occupied positions of a triangular lattice in different colors (gray levels) with various coverages. Fig. 1 shows not only the basic lattice hexagon (dark) but also adjacent hexagons (light) with identical configurations representing the periodic boundary conditions. The interaction in this section is described by (2.1) and (2.2). Fig. 2.a acts as reference to [3] with a coverage $\theta=0.045$ to demonstrate that the new algorithm leads to the same sample results. A substrate aligned superlattice of adatoms and a few dimers with a lattice parameter of 5 grid units shows up like in the reference.

The adatom pair distribution in a 30 degree sector taken from a configuration average is shown in Fig. 2.b. Dots with different colors/ darkness at lattice

positions mark Pair distribution ranges:

- $g_{ik} \geq 1.5$ black
- $1.5 > g_{ik} \geq 1.0$ blue/ dark grey
- $1.0 > g_{ik} \geq 0.5$ green/ medium gray
- $g_{ik} > 0.5$ yellow/ light gray.

Black points at 5 and 10 lattice spacings in the $\langle 1-10 \rangle$ direction and at $5\sqrt{3}$ in the $\langle 1-21 \rangle$ direction reflect the aligned monomer superlattice. We note a light dot at 1 lattice spacing in the $\langle 1-10 \rangle$ direction reflecting almost no population of next neighbor sites.

3.2. Influence of Substrate Elastic (An-)Isotropy

Previous investigations showed a strong influence of the substrate elastic constants on the adatom pair distribution [5]. A triangular grid algorithm could compromise such delicate matter. To prove the grid algorithm properly handling substrate isotropy, the elastic constants of tungsten were used as reference (see Tab.1). Fig.3 shows the resulting pair distribution for a coverage $\theta=0.045$ in a 30 degree sector. It shows the characteristic rings at 5 lattice spacings already discussed in [5].

Isotropy could also be compromised by adatom dipoles or multipoles. Though there are almost no angular moments of circular clusters in the relevant distance of 5 lattice constants, adatom straight tripoles would generate differences in the interaction of up to 18% (less repulsive orthogonal to the axes).

3.3. Adatom Configurations for Coverages between 0.1 and 1 Monolayer

To stay consistent with [3] and with experimental observations of monomer superstructures [9,10] we will stay in this section with short range interaction $U_1(s, \phi)$ (2.2) and thus with the more repulsive variant 1. In 0.1 steps the coverage is increased in Figs. 4.a..p showing the effects of a subsequent population of the 2-dimensional triangular lattice up to 0.9 monolayers and the corresponding pair distributions according to (2.6) up to a coverage of 0.5 monolayers (coverages beyond 0.5 will be treated separately below).

Fig.4.a shows a sample configuration at coverage $\theta=0.1$ and Fig.4.b shows the equivalent pair distribution taken from a configuration average. The black dots in Fig.4.b at $s_{\langle 1-10 \rangle}=5$ and $s_{\langle 1-21 \rangle}=5\sqrt{3}$ indicate a superlattice with a superlattice constant of 5 consisting of dimers, trimers and a few 4-mers. The dark dot at $s_{\langle 1-10 \rangle}=1$ reflects the high amount of next neighbors.

Fig.4.c shows a sample configuration at coverage $\theta=0.2$ and Fig.4.d shows the equivalent pair distribution taken from a configuration average. The black dots in Fig.4.d at $s_{\langle 1-10 \rangle}=4 / 5$ and the dark dots at $s_{\langle 1-10 \rangle}=9$ to 10 and $s_{\langle 1-21 \rangle}=5\sqrt{3}$ indicate an island superlattice, now with a superlattice constant of $4 / 5$ consisting of Nmers and some smaller aggregates.

Fig.4.e shows a sample configuration at coverage $\theta=0.3$ and Fig.4.f shows the equivalent pair distribution taken from a configuration average. The black dots

in Fig.4.f at $s_{\langle 1-10 \rangle} = 5$ and the dark dots at $s_{\langle 1-10 \rangle} = 10$ and $s_{\langle 1-21 \rangle} = 5\sqrt{3}$ again indicate a superlattice, now with a superlattice constant of 5 consisting of circular and elongated Nmers.

Fig.4.g shows a sample configuration at coverage $\theta=0.4$. Many elongated islands, connected by thin bridges, have formed. Fig.4.h shows the equivalent pair distribution taken from a configuration average. g_{ik} values of 1.35 at $s_{\langle 1-10 \rangle} = 4/5$ indicate weak island alignment in the $\langle 1-10 \rangle$ directions and a characteristic distance of $4/5$.

Fig.4.i shows a sample configuration at coverage $\theta=0.5$. The elongated islands of Fig.4.g have now merged to an interwoven stripe structure. Fig.4.j shows the equivalent pair distribution taken from a configuration average. g_{ik} values of 1.3 at $s_{\langle 1-10 \rangle} = 4/5$ indicate weak stripe alignment in the $\langle 1-10 \rangle$ directions and a characteristic distance of $4/5$.

Fig.4.k shows a sample configuration at coverage $\theta=0.6$. The occupied stripes have grown thicker and the vacancies have lost connectivity.

Fig.4.l shows a sample configuration at coverage $\theta=0.7$. The vacancies have reduced to islands forming a superlattice inverse to the one in Fig.4.e.

Fig.4.m shows a sample configuration at coverage $\theta=0.8$. The vacancies are forming aligned clusters like the adatoms in Fig.4.c.

Fig.4.n shows a sample configuration at coverage $\theta=0.9$. The vacancies are forming aligned dimers, trimers, Nmers like the adatoms in Fig.4.a.

Fig.4.o shows a sample configuration at coverage $\theta=0.955$. The vacancies show almost a monomer superlattice like the adatoms in Fig.2.a.

Omitting the pair distributions for coverages $\theta > 0.5$ has a good reason: they have almost constant values and no clear structure. To verify the observation of vacancy structures at $\theta > 0.5$ inverse to adatom structures at $\theta < 0.5$, a vacancy pair distribution

$$g_{ik}^{\text{vac}} = \langle (1 - \tau_i)(1 - \tau_k) \rangle / (1 - \rho)^2, \quad (3.1)$$

is introduced. g_{ik}^{vac} measures the likeliness of vacancy pairs $\{(1-\tau_i), (1-\tau_k)\}$. Fig.4.p shows the vacancy pair distribution taken from a configuration average at coverage $\theta=0.9$. It shows almost the same structure as the adatom pair distribution at coverage $\theta=0.1$ in Fig.4.b, indicating a superlattice now of vacancy dimers and trimers and some Nmers.

In summary the interaction u_1 with increasing coverage leads to clusters growing on superlattice positions from mono- to N-mers. Subsequently elongated islands are formed, merge to stripes at 0.5 ML and then the sequence is reversed with empty positions instead of occupied ones. Such changes in adatom morphology are summarized in Tab.2.

Coverage	Form	Superlatt.	Invers.	Adatoms	Vacancies	FeatureSize
\square	\square	\square	\square	avg.	avg.	avg.
0.045	mono	Y	\square	1	\square	5
0.1	di	Y	\square	2	\square	4.8
0.2	cluster	Y	\square	4	\square	4.6
0.3	round/linear	Y	\square	7	\square	4.8
0.4	elongated/connected	\square	\square	9	\square	4.7
0.5	coherentstripes	\square	\square	\square	\square	4.6
0.6	elongated/connected	\square	Y	\square	9	\square
0.7	round/linear	Y	Y	\square	7	\square
0.8	cluster	Y	Y	\square	4	\square
0.9	di	Y	Y	\square	2	\square
0.955	mono	Y	Y	\square	1	\square

Table 2. Changes of adatom morphology with increasing coverage, Monte-Carlo simulated with interaction u_1

3.4. Influence of Short Range Interactions

Variant 1 $U_1(s, \phi)$ (2.2) of the short range interaction was used in [3] to enable convergence of the BGY type integral equation. Compared with (2.1) it describes an effective repulsive interaction in the short range. To show the influence of short range interactions, variant 2 $U_2(s, \phi)$ (2.3) is chosen less repulsive and therefore promotes adatoms to nucleate at next neighbor sites. We note in the pair distributions below black or dark dots at next neighbor distance.

Fig.5.a shows a sample configuration with short range interaction $U_2(s, \phi)$ (2.3) at coverage $\theta=0.045$ and Fig.5.b shows the equivalent pair distribution taken from a configuration average. Compared with Figs.2.a,b the superlattice is maintained but now consists of more dimers, trimers and some Nmers and the black dots at $s_{<1-10>}=6$ and 12 and $s_{<1-21>}=6*\sqrt{3}$ reflect a superlattice constant of 6.

Fig.5.c shows a sample configuration with short range interaction $U_2(s, \phi)$ (2.3) at coverage $\theta=0.1$. The superlattice consists of many Nmers and some smaller aggregates. Fig.5.d shows the equivalent pair distribution taken from a configuration average. The black dots at $s_{<1-10>}=5/6$ and the dark dots 11 at $s_{<1-21>}=6*\sqrt{3}$ again indicate a superlattice, now with a lattice constant of $5/6$.

Fig.5.e shows a sample configuration with short range interaction $U_2(s, \phi)$ (2.3) at coverage $\theta=0.3$. The superlattice consists of islands some of which have merged to elongated islands. Small bridges between islands create dog-bone-like shapes. Fig.5.f shows the equivalent pair distribution taken from a configuration average. g_{ik} values of 1.4 at $s_{<1-10>}=6$ indicate a weak superlattice, aligned in the $<1-10>$ directions and a characteristic distance of 6. There is also a trend towards isotropy indicated by an emerging ring structure at a distance of 6.

Fig.5.g shows a sample configuration with short range interaction $U_2(s, \phi)$ (2.3) at coverage $\theta=0.5$. The islands of lower coverages have now merged to an interwoven but incoherent stripe structure with an average stripe broadness of 3. Fig.5.h shows the equivalent pair distribution taken from a configuration average. g_{ik} values of 1.1 at $s=5/6$ in all directions indicate isotropy. Compared with Fig. 4.e - with short range interaction U_1 at $\theta=0.5$ - the stripes are a bit thicker, less coherent and their distance is about one lattice constant larger.

Variant 3 $U_3(s, \phi)$ (2.4) is more attractive and therefore strongly promotes adatoms to nucleate at next neighbor sites. We note in the pair distributions black dots at 1 lattice spacing in the $<1-10>$ direction reflecting strong population of next neighbor sites.

Fig.5.i shows a sample configuration with short range interaction $U_3(s, \phi)$ (2.4) at coverage $\theta=0.045$. Compared with Fig.2.a there are much more dimers and trimers and the medium range order is much lower. Fig.5.j shows the equivalent pair distribution taken from a configuration average. The black dot at $s_{<1-10>}=5/6$ reflects a superlattice constant of $5/6$ but the missing black dots at increased distances confirm a reduced order.

Fig.5.k shows a sample configuration with short range interaction $U_3(s, \phi)$ (2.4) at coverage $\theta=0.1$. The cluster structure consists of all kinds of sizes from monomers to Nmers. Fig.5.l shows the equivalent pair distribution taken from a configuration average. g_{ik} values of 1.3 at $s=5/6$ in all directions indicate isotropy, i.e. a reduced alignment to the substrate crystal directions compared to Figs.4.a and 5.c.

Fig.5.m shows a sample configuration with short range interaction $U_3(s, \phi)$ (2.4) at coverage $\theta=0.3$. The cluster structure consists of larger islands some of which have merged to elongated islands. A few small bridges between islands create dog-bone-like shapes. Fig.5.n shows the equivalent pair distribution taken from a configuration average. g_{ik} values of 1.1 at $s_{<1-10>}=5/6$ and of 1.2 at $s_{<1-21>}=3*\sqrt{3}$ indicate almost isotropic rings with a characteristic distance between 5 and 6.

Fig.5.o shows a sample configuration with short range interaction $U_3(s, \phi)$ (2.4) at coverage $\theta=0.5$. The islands of lower coverages have merged to an interwoven but incoherent stripe structure with an average stripe broadness of 3. Fig.5.p shows the equivalent pair distribution taken from a configuration average. g_{ik} values of 1.05 at $s_{<1-10>}=5/6$ and of 1.1 at $s_{<1-21>}=3*\sqrt{3}$ indicate very weak isotropy with rings of a characteristic distance between 5 and 6. Compared with Fig. 5.g - with short range interaction U_2 at $\theta=0.5$ - the stripes look similar, but if Fig.5.p is compared with Fig.5.h we note a weak tendency towards a $<1-21>$ alignment in the U_3 case.

In summary the more attractive variants lead to less ordered superlattices consisting of more adatoms with a greater superlattice constant and thicker, less coherent stripes.

4. Discussion

4.1. Model Assumptions

Many assumptions and approximations used for this model have been discussed in [3] in detail. The most relevant approximation is an elastic continuum model for the substrates instead of a lattice model, known to be inadequate for describing short range effects. The elastic continuum model predicts a s^{-3} repulsion on the long range, a repulsive wall near 2.3 lattice distances and a strong attractive well at next neighbor distances.

Replacement of the deep attractive potential well by either a cap of about 5 units (in fact describing a weak repulsion of next neighboring adatoms) or by a cap at potential zero (in fact describing a weak attraction of next neighboring adatoms) or by a cap at potential -5 units (describing a stronger attraction of next neighbors) is a method to indicate the effects of short range interactions while preserving the merits of a theory with medium range focus.

4.2. Adatom Distribution on Cu $\langle 111 \rangle$

The results of sections 3.1 to 3.3 draw the picture of a substrate aligned hexagonal dense packed superlattice of adatoms or clusters at coverages up to $\theta \approx 0.3$ ML, stripes around coverages $\theta = 0.5$, and of a substrate aligned dense packed superlattice of vacancies or vacancy clusters beyond $\theta \approx 0.7$ ML. The Monte-Carlo simulations predict a populated/unpopulated symmetry $\theta/(1-\theta)$. This is explained by minimization of the total configuration energy by forming adatom clusters or stripes or vacancies around 5 lattice distances apart. Substrate strain generated by adatoms stressing the surface is allowed to release within the unpopulated sites.

4.3. Comparison with previous off-grid Simulations

The adatom configurations with interaction U_1 at $\theta = 0.045$ resulting from an off-grid algorithm in [3] could be repeated with an on-grid algorithm. Both results and the derived pair distributions are consistent with the solution of a Born-Green-Ivon type integral equation describing the adatom pair distribution from Statistical Mechanics principles [3,6]. So the present Monte-Carlo simulations can be rated as a high coverage extension of previous results.

4.4. The Role of Short Range Interactions

The results of section 3.4 indicate a strong role of short range interactions. In short they drive trends towards

- larger clusters
- circular clusters
- less connected clusters
- less influence of the substrate on the superlattice directions, i.e. isotropy
- increased feature size.

The unexpected nearly constant feature sizes for one type of short range interactions within a wide range of coverages (see Tab. 2) also seems to be related to short range interactions.

4.5. Comparison with Experiments and the Influence of Temperature

Strain mediated superlattices on Cu<111> in the coverage region up to $\theta=0.045$ ML were already discussed and compared with experiments [9,10] in [3]. The agreement was good enough to propose strain mediated interactions as an alternative to the one discussed in [9,10]. The current investigation was triggered by an unknown referee of [5]. He raised the point how other manifestations of elastic interactions on surfaces, especially stress domains [11], are related to adatom superstructures.

Stress domains are ordered patterns of less dense and more dense adatom areas, for example adatom gas areas and monolayer areas forming spontaneously. They minimize surface energy by balancing short-range attractive with long-range repulsive interaction. Substrate strain created by surface stress in the more dense areas is allowed to relax in the less dense areas. The domains reflect the elastic anisotropy of the substrate.

The observations at the Pb/Cu<111> system [4] can be characterized by

- ordered but mobile circular droplets (containing thousands of adatoms) at low coverages
- stripes at medium coverage with a long range order improving when reducing temperature
- ordered inverse droplets at high coverages approaching a monolayer (as predicted earlier, see references in [4]).

The periodicity of patterns is in the 100 nm range, decreasing with increasing temperature. The observed temperature range is 623 K to 673 K. The order of droplets can - from a first glance - be interpreted as a superlattice type.

The beautiful sequence of island superlattices, domain patterns and inverse droplets on Pb/Cu<111> with increasing coverage observed in [4] would serve as a striking experimental evidence of the theory and the simulation results presented in section 3.4 if the length scales and the temperature would be the same. Unfortunately [4] describes a high temperature experiment with adatom clusters of thousands of adatoms while the experiments showing superlattice effects on a few lattice constant scale have been performed in the 10K region [9,10]. So the question arises if the present Monte-Carlo simulation could be extended to handle clusters and structures of hundreds or thousands of adatoms. Unfortunately this would be far beyond the resources of a PC, so we must rely

on scaling arguments to argue the same driver - elastic interactions - for both phenomena, adatom superlattices and stress domain patterns:

Following the cluster section of [7] we argue a simple superposition ansatz for the elastic interactions: two clusters of n_1 and n_2 adatoms create $n_1 * n_2$ times the elastic inter cluster energy of two single adatoms. This ansatz, of course, is a strong restriction not considering e.g. lattice mismatch effects. Anyhow it could be valid for the case Pb/Cu<111> if short range adatom-adatom interactions would not dominate. Equation (2.7) could then be interpreted as interaction between n adatom clusters with $U_0^{\text{Cluster}} = n^2 U_0$.

A $n=10^3$ cluster would create an interaction U_0^{Cluster} 10^6 times U_0 . The temperature range for the stress domain experiments at 650 K is a factor 10^2 higher than the regime of single adatom effects, so the scaled cluster interaction $u_0^{\text{Cluster}} = U_0^{\text{Cluster}} / k_B T$ would be 10^4 times higher. The typical length s_0^{Cluster} according to eq. (2.8) would then be $10^{4/3} \approx 21$ times higher than s_0 . The coverage θ^{Cluster} would be reduced by a factor of about 8 (noting that the coverage of adatoms and of clusters have different meaning).

We can summarize that length scales may differ from 5 substrate lattice constants to 100 lattice constants in the example above, but the elastic interaction mechanism is the same.

It would be a big surprise if some simple scaling arguments could explain the physics of stress domains more than qualitatively. In fact the measurement in [14] show a decrease in domain feature size from 140 nm to 40 nm when the temperature rises from 590 K to 650 K, far beyond the above scaling effects. The authors explain such decrease in stripe periodicity with the change in domain-boundary free energy caused by thermally broken Pb-Pb bonds. Thus the effects of short range interactions override the effects of elastic medium range interactions under certain conditions. This is not in contradiction to the scaling arguments above since eq. (2.8) is valid only for a s^{-3} type interaction which does not include short range effects.

The influence of substrate anisotropy as observed in [12] is reflected in the present Monte-Carlo simulations and the pair distributions derived. However the dominating stripe orientations reported at coverage $\theta=0.5$ ML are <-1-12> directions, found within the simulations only for the stronger short range attractive interaction U_3 .

Equilibrium conditions are confirmed by experiments with reversible shape transitions (droplet to elongated islands with dog-bone-like shapes) during heating cycles [13]. An increase in temperature changes the shapes the same way as an increasing coverage does, again in line with the scaling arguments outlined above (same shape of $g(s, u_0, \theta)$ if u_0 reduced or θ increased). Both experimental results can be seen as a hint for the validity of the assumptions and conclusions.

4.6. Open Questions

The prime question is about the existence of clusters arranged in superlattices and of stress domain patterns on Cu<111> in the temperature range of about

10K and with a characteristic length of about 5 to 6 lattice constants. Such structures may be found in material already measured. Similar important questions are the size and nature of short range interactions and especially the reasons for different stripe orientations. More experimental material is needed to determine size and nature of short range interactions and also the orientation of cluster/ stripe structures relative to the substrate crystal directions. Also lattice type theories need to be applied for a better understanding. A further important question is how the theory successfully describing mesoscopic stress patterns [11] can be utilized to better understand the microscopic effects discussed in the present analysis - if domain boundary effects play an important role in the mesoscopic range, the effects of short range interactions in the microscopic range should be even more significant.

Nothing was said about the influence of adatom elements on the morphology. Adatoms will differ in their stress parameter P and in their short range interactions. While differences in P should change only the temperatures in which effects like superlattices are observable, differences in their short range interaction can change the morphology. As example of the latter we refer to section 3.4 where superlattices of single adatoms were not observed at all due to a more attractive short range potential.

The morphology of adatoms on other surfaces like $\text{Cu}\langle 001 \rangle$ or other substrates is an equally interesting topic, the much stronger elastic anisotropy of $\langle 001 \rangle$ surfaces of many materials is expected to lead to further insight. Increasing the accuracy of the simulation by increasing the diameter of the simulation area on much more powerful computers may also lead to additional insights.

7. Summary

Substrate strain mediated adatom configurations have been Monte-Carlo simulated for $\text{Cu}\langle 111 \rangle$ surfaces for three short range interaction types. The adatom coverages range up to nearly a monolayer. Pair distributions have been derived and prove morphologies from superlattices of single adatoms and clusters to ordered stress domain patterns. Higher coverages beyond 0.5 monolayers show vacancy structures just inverted. The short range interaction shows a significant influence on the cluster size within the superlattices. Substrate elastic anisotropy strongly influences the superlattice orientation with respect to the substrate crystal directions.

Experimentally a quite similar behavior has been published. For low temperatures superlattices of single adatoms have been reported while for high temperatures ordered islands and stripes of thousands of adatoms have been reported. There is some evidence of elastic interactions being the common cause but a final conclusion on the validity of the theory remains open at this point in time.

References

- [1] H.Brune, Creating Metal Nanostructures at Metal Surfaces Using Growth Kinetics, in: Handbook of Surface Science Vol.3 (E.Hasselbrink and B.I.Lundqvist ed.), Elsevier, Amsterdam (2008)
- [2] H.Ibach, Surf.Sci.Rep. 29, 195 (1997)
- [3] W.Kappus, arXiv:1205.2480
- [4] R.Plass, J.A.Last, N.C.Bartelt, G.L.Kellogg, Nature 412, 875 (2001)
- [5] W.Kappus, arXiv:1203.2240 (2012)
- [6] W.Kappus, J.Phys.C: Solid State Phys. 11, L565 (1978)
- [7] W.Kappus, Z.Physik B 29, 239 (1978)
- [8] A.G.Every, A.K.McCurdy: Table 3. Cubic system. Elements. D.F.Nelson(ed.), SpringerMaterials- The Landolt-Börnstein Database
- [9] J. Repp, F. Moresco, G. Meyer, K. H. Rieder, P. Hyldgaard and M. Persson, Phys. Rev. Lett. 85, 2981 (2000).
- [10] F. Silly, M. Pivetta, M. Ternes, F. Patthey, J.P. Pelz, W.D. Schneider, New J. of Phys. 6, 16 (2004)
- [11] O.L.Alerhand, D.Vanderbilt, R.D.Meade, J.D.Joannopoulos, Phys. Rev. Lett. 61, 1973 (1988)
- [12] F.Leonard, N.C.Bartelt, G.L.Kellogg, Phys. Rev. B 71, 045416 (2005)
- [13] R.van Gastel, N.C.Bartelt, G.L.Kellogg, Phys. Rev. Lett. 96, 036106 (2006)
- [14] R.van Gastel, N.C.Bartelt, P.J.Feibelman, F.Léonard, and G.L.Kellogg, Phys. Rev. B 70, 245413 (2004)

Acknowledgement

Many thanks to the unknown referee of [5] for directing the author's interest to stripes.

Appendix

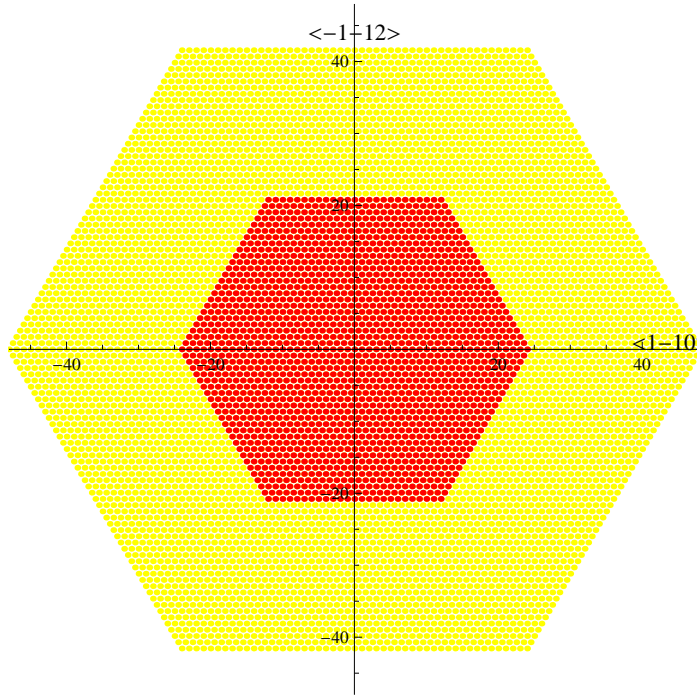


Fig. 1 shows the basic lattice hexagon and adjacent hexagons representing the periodic boundary conditions.

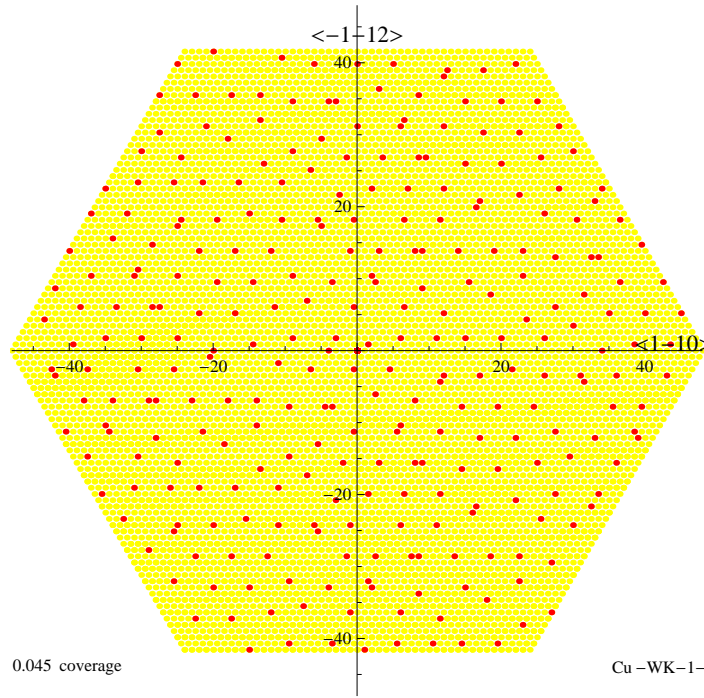


Fig. 2.a shows a sample configuration with reference short range interaction $U_1(s, \phi)$ (2.2) and a coverage $\theta=0.045$.

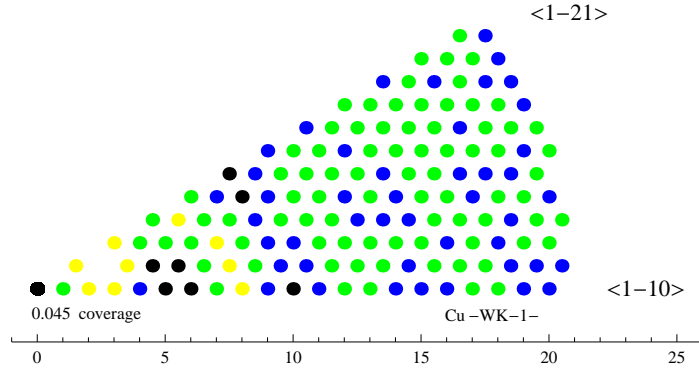


Fig. 2.b shows an average adatom pair distribution in a 30 degree sector with reference short range interaction $U_1(s, \phi)$ (2.2) and a coverage $\theta=0.045$. The differently colored dots represent different values of the pair distribution (darker colors represent higher values).

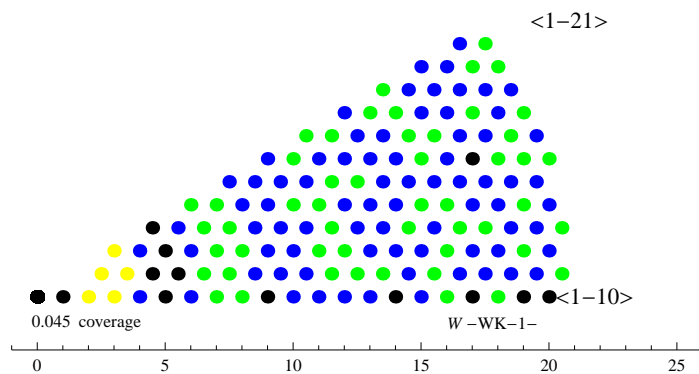


Fig.3 shows an average pair distribution for an isotropic substrate (tungsten) at coverage $\theta=0.045$ in a 30 degree sector.

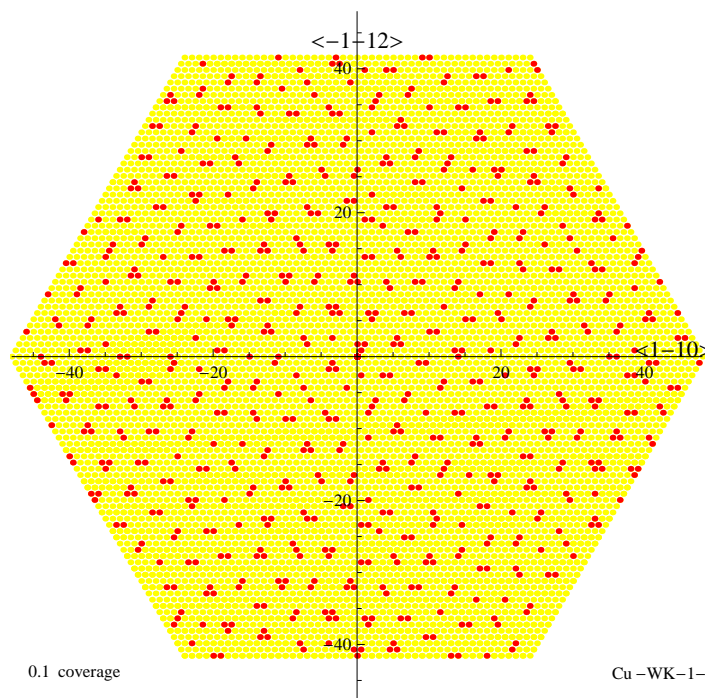


Fig.4.a shows a sample configuration with short range interaction $U_1(s, \phi)$ (2.2) at coverage $\theta=0.1$.

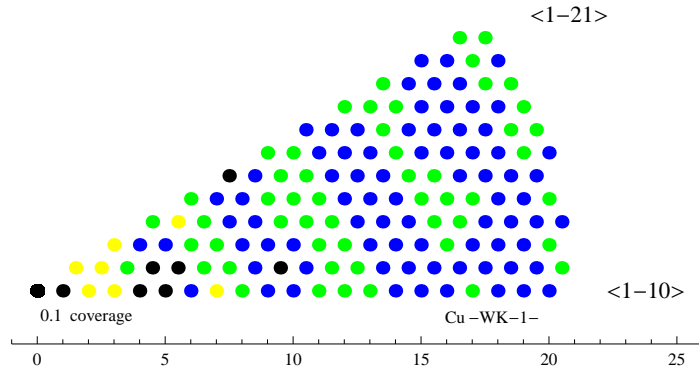


Fig.4.b shows an average pair distribution with short range interaction $U_1(s, \phi)$ (2.2) at coverage $\theta=0.1$.

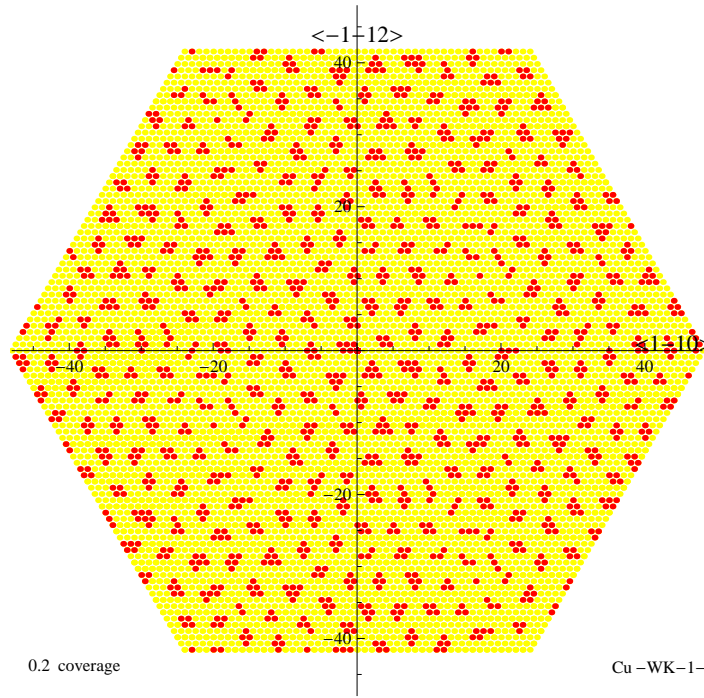


Fig.4.c shows a sample configuration with short range interaction $U_1(s, \phi)$ (2.2) at coverage $\theta=0.2$.

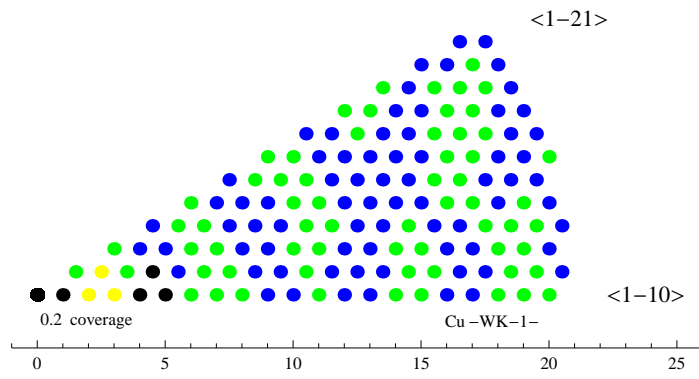


Fig.4.d shows an average pair distribution with short range interaction $U_1(s, \phi)$ (2.2) at coverage $\theta=0.2$.

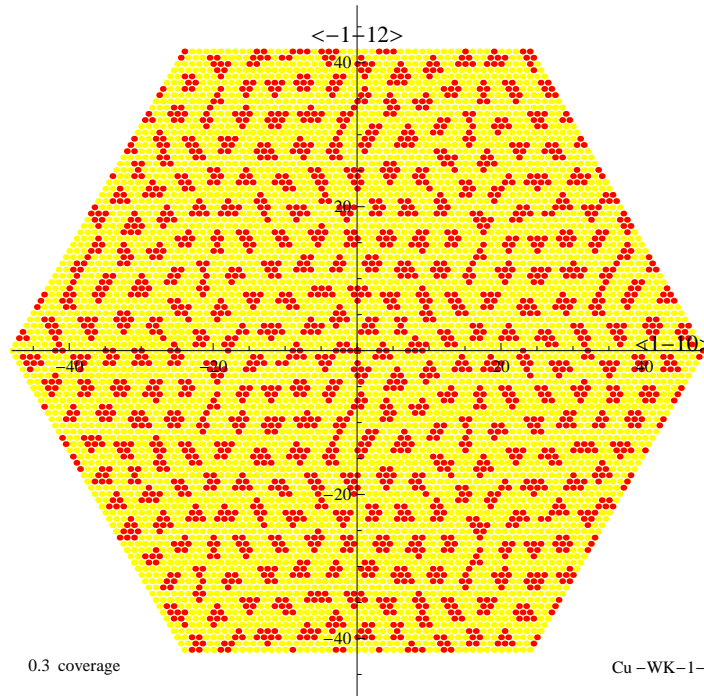


Fig.4.e shows a sample configuration with short range interaction $U_1(s, \phi)$ (2.2) at coverage $\theta=0.3$.

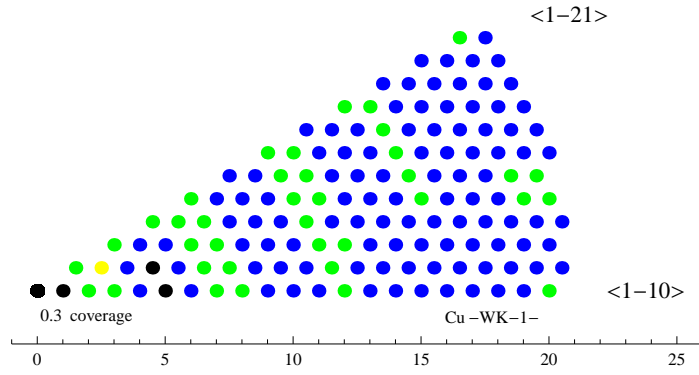


Fig.4.f shows an average pair distribution with short range interaction $U_1(s, \phi)$ (2.2) at coverage $\theta=0.3$.

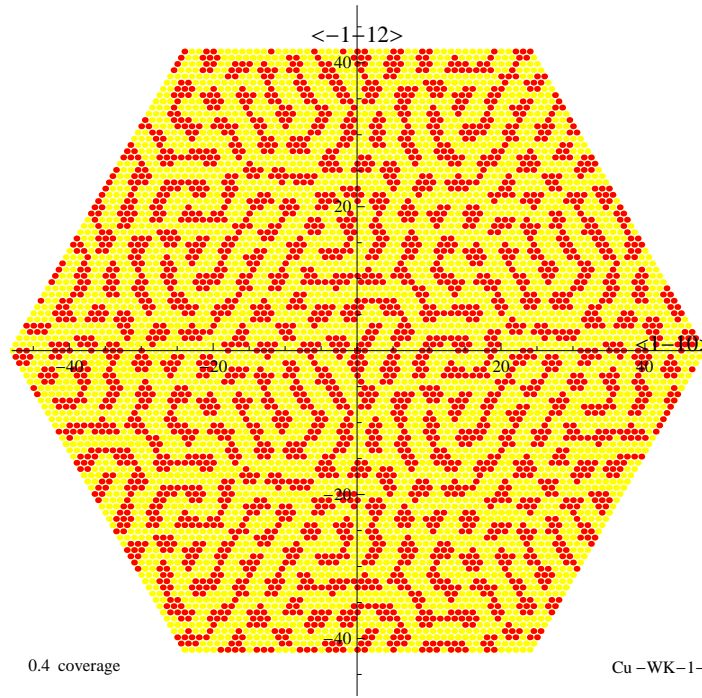


Fig.4.g shows a sample configuration with short range interaction $U_1(s, \phi)$ (2.2) at coverage $\theta=0.4$.

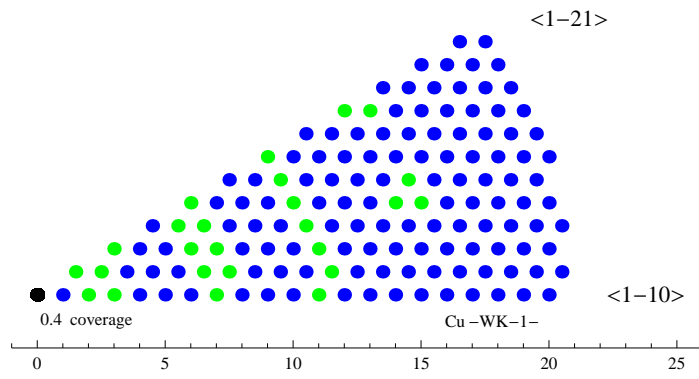


Fig.4.h shows an average pair distribution with short range interaction $U_1(s, \phi)$ (2.2) at coverage $\theta=0.4$.

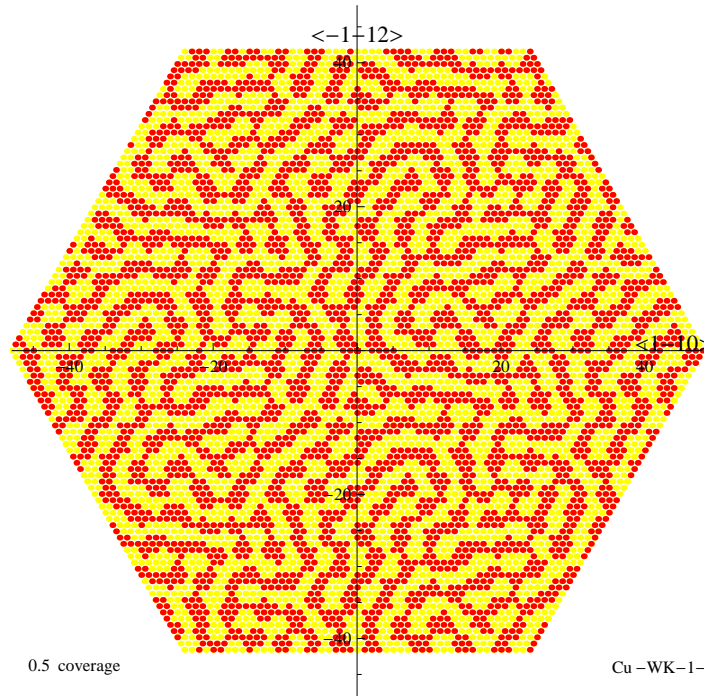


Fig.4.i shows a sample configuration with short range interaction $U_1(s, \phi)$ (2.2) at coverage $\theta=0.5$.

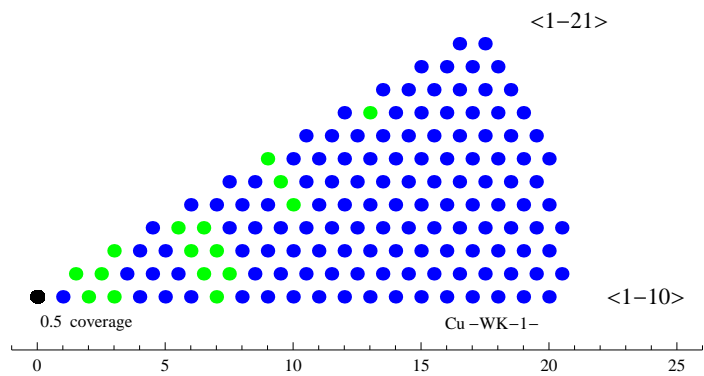


Fig.4.j shows an average pair distribution with short range interaction $U_1(s, \phi)$ (2.2) at coverage $\theta=0.5$.

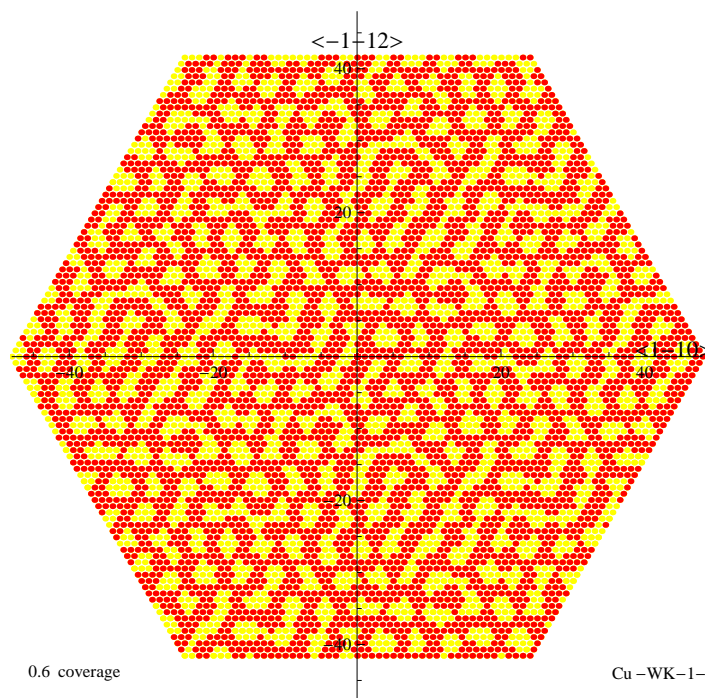


Fig.4.k shows a sample configuration with short range interaction $U_1(s, \phi)$ (2.2) at coverage $\theta=0.6$.

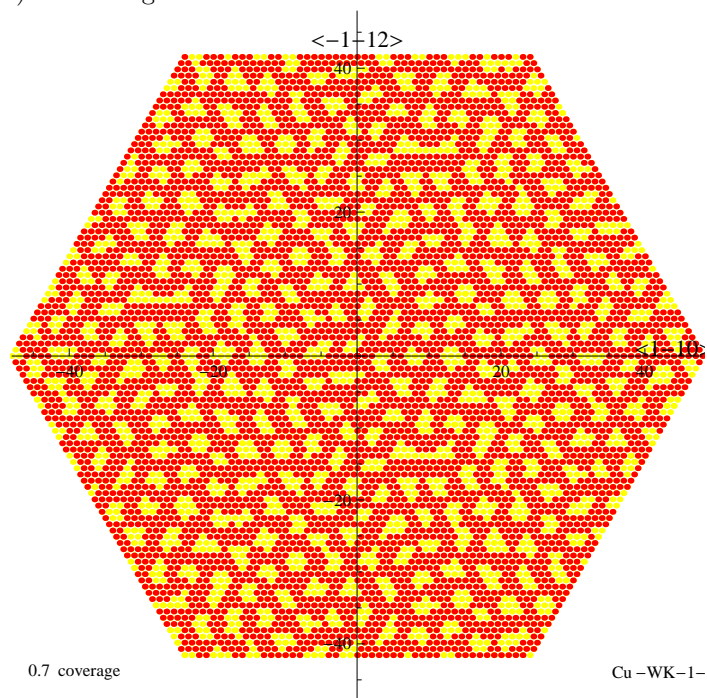


Fig.4.l shows a sample configuration with short range interaction $U_1(s, \phi)$ (2.2) at coverage $\theta=0.7$.

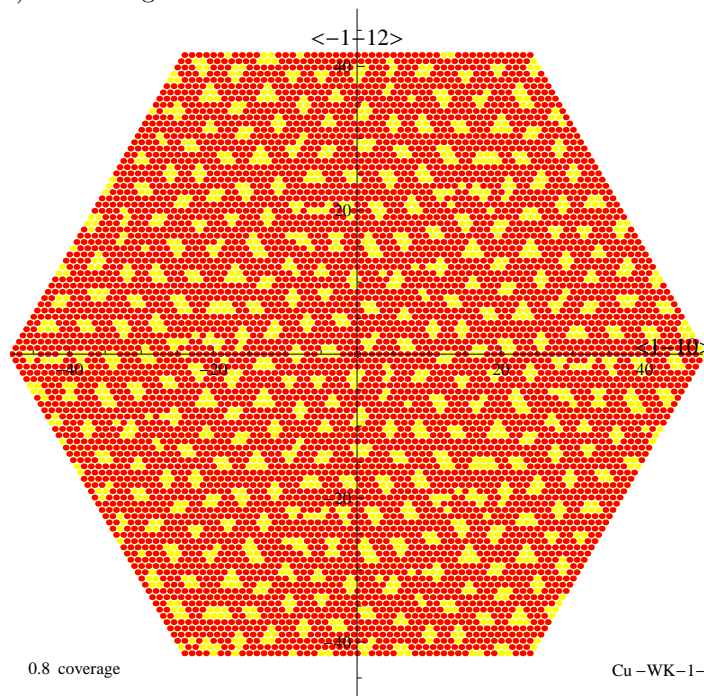


Fig.4.m shows a sample configuration with short range interaction $U_1(s, \phi)$ (2.2) at coverage $\theta=0.8$.

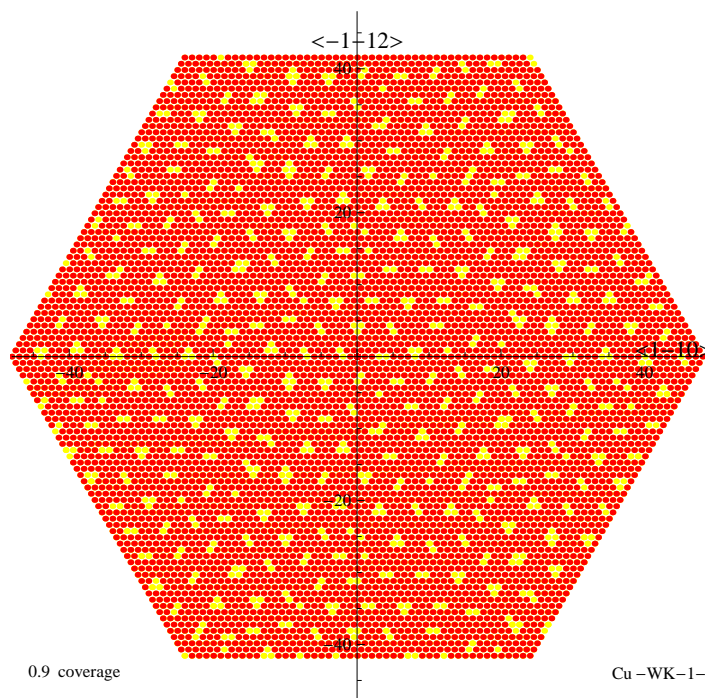


Fig.4.n shows a sample configuration with short range interaction $U_1(s, \phi)$ (2.2) at coverage $\theta=0.9$.

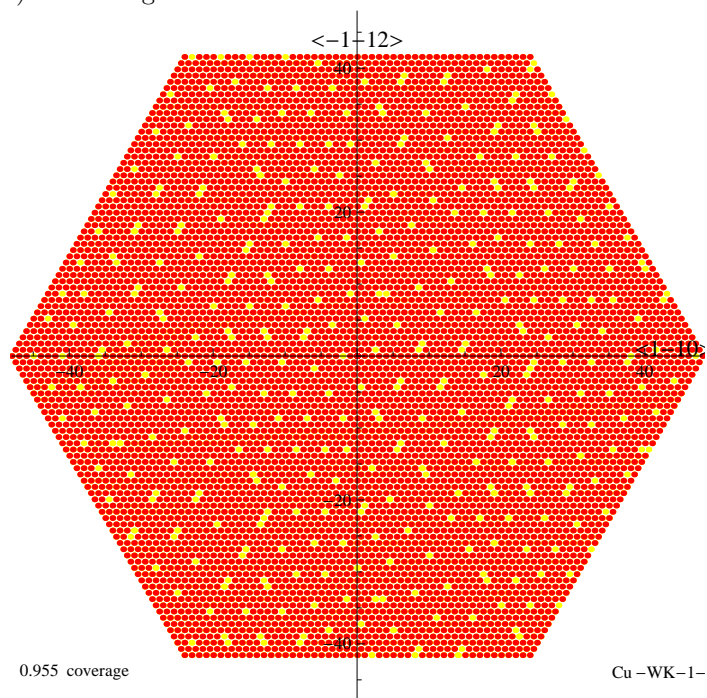


Fig.4.o shows a sample configuration with short range interaction $U_1(s, \phi)$ (2.2) at coverage $\theta=0.955$.

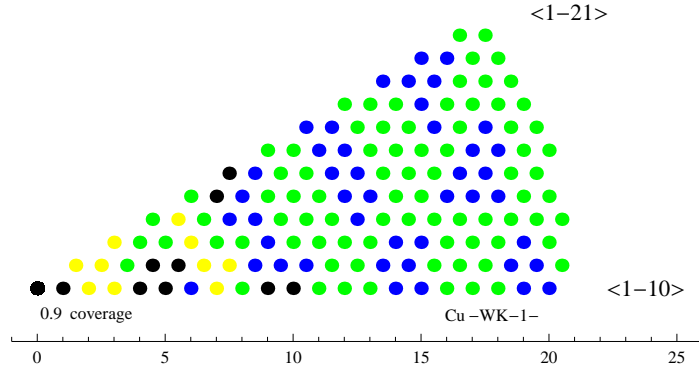


Fig.4.p shows an average vacancy pair distribution (3.1) with short range interaction $U_1(s, \phi)$ (2.2) at coverage $\theta=0.9$.

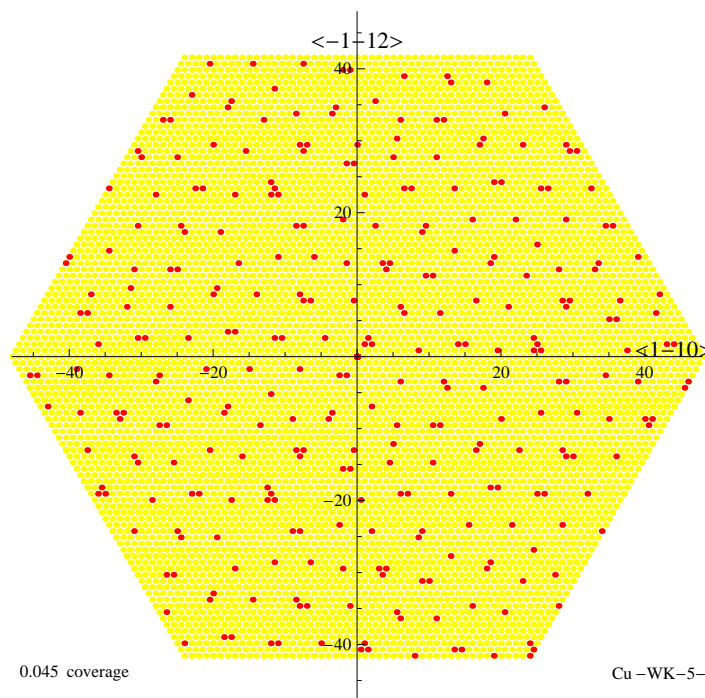


Fig.5.a shows a sample configuration with short range interaction $U_2(s, \phi)$ (2.3) at coverage $\theta=0.045$.

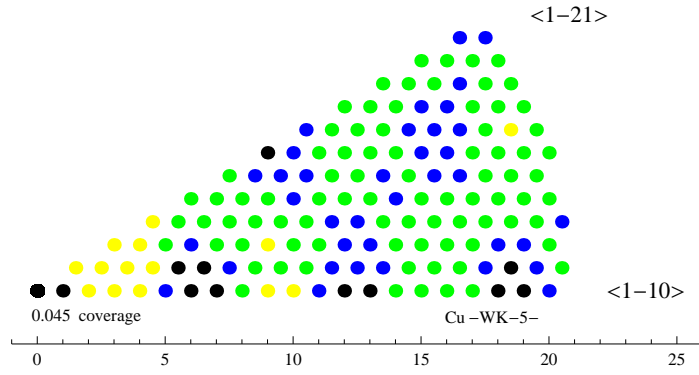


Fig.5.b shows an average pair distribution with short range interaction $U_2(s, \phi)$ (2.3) at coverage $\theta=0.045$.

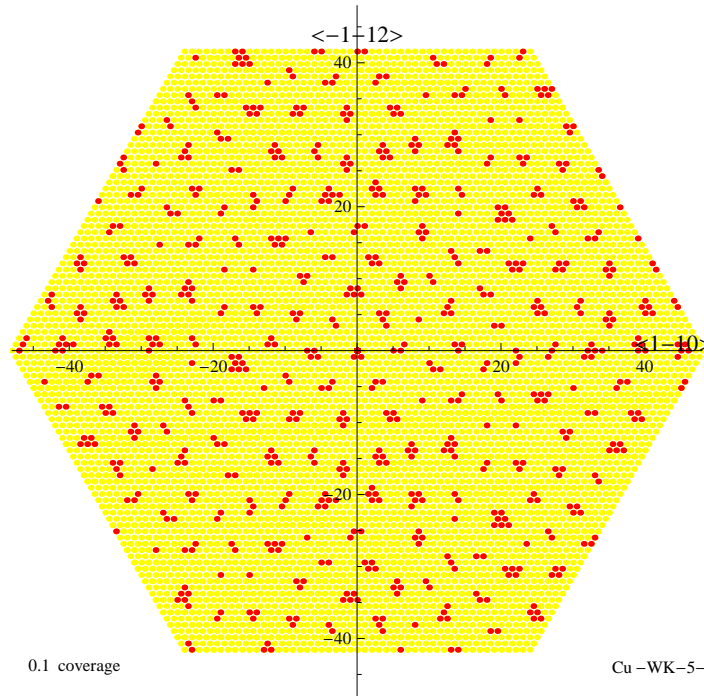


Fig.5.c shows a sample configuration with short range interaction $U_2(s, \phi)$ (2.3) at coverage $\theta=0.1$.

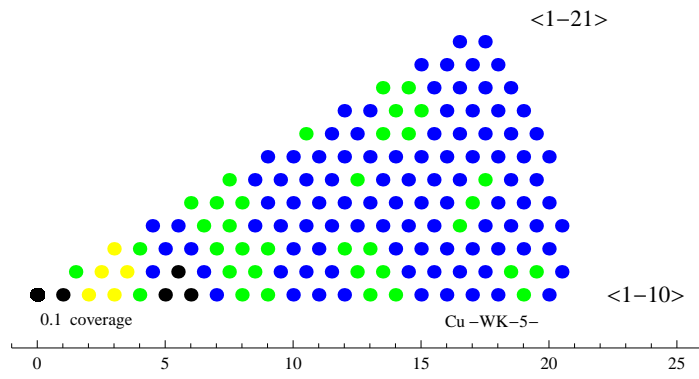


Fig.5.d shows an average pair distribution with short range interaction $U_2(s, \phi)$ (2.3) at coverage $\theta=0.1$.

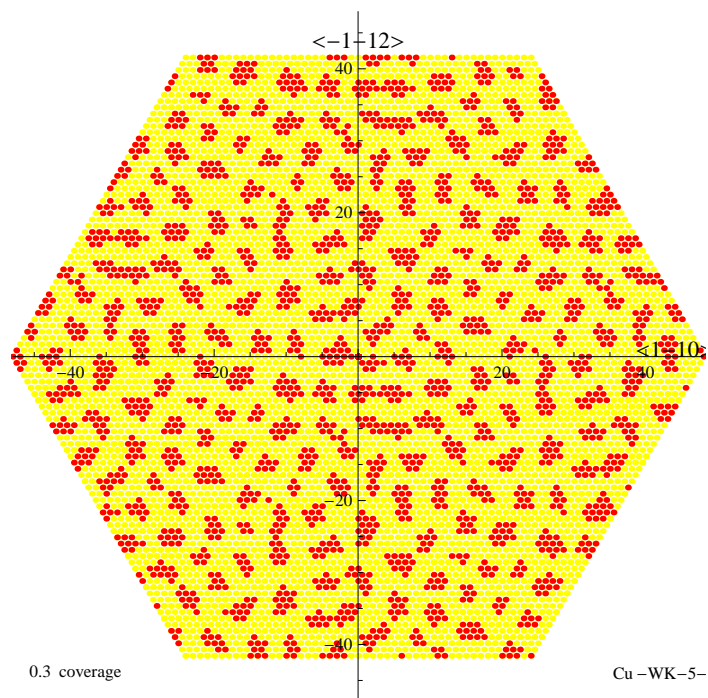


Fig.5.e shows a sample configuration with short range interaction $U_2(s, \phi)$ (2.3) at coverage $\theta=0.3$.

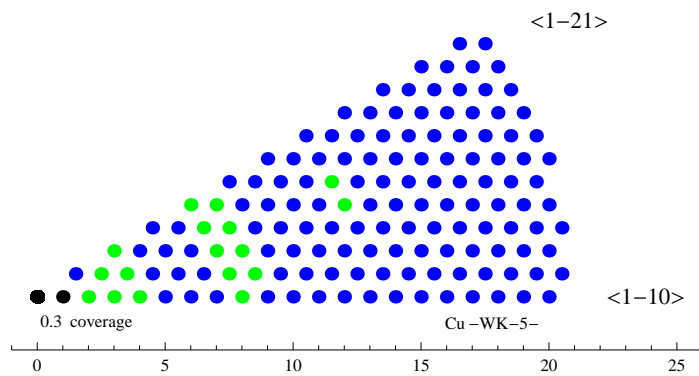


Fig.5.f shows an average pair distribution with short range interaction $U_2(s, \phi)$ (2.3) at coverage $\theta=0.3$.

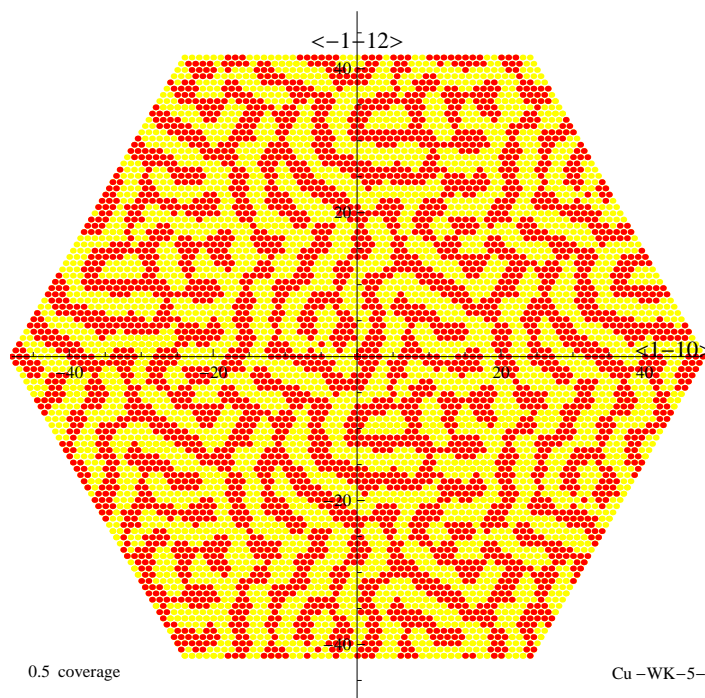


Fig.5.g shows a sample configuration with short range interaction $U_2(s, \phi)$ (2.3) at coverage $\theta=0.5$.

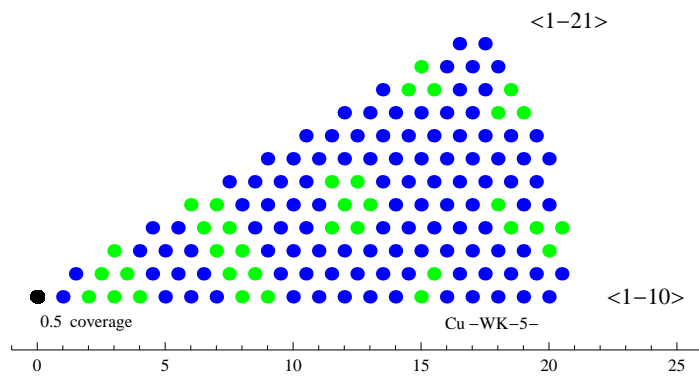


Fig.5.h shows an average pair distribution with short range interaction $U_2(s, \phi)$ (2.3) at coverage $\theta=0.5$.

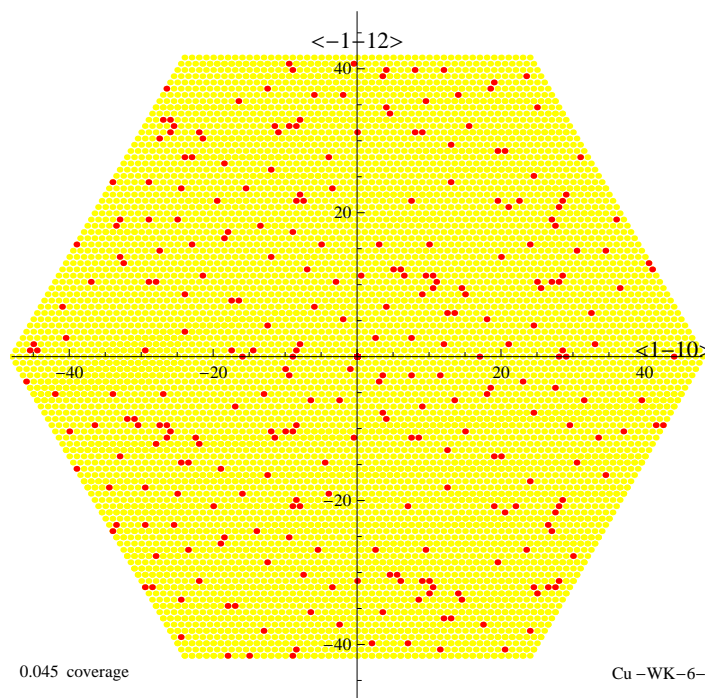


Fig.5.i shows a sample configuration with short range interaction $U_3(s, \phi)$ (2.3) at coverage $\theta=0.045$.

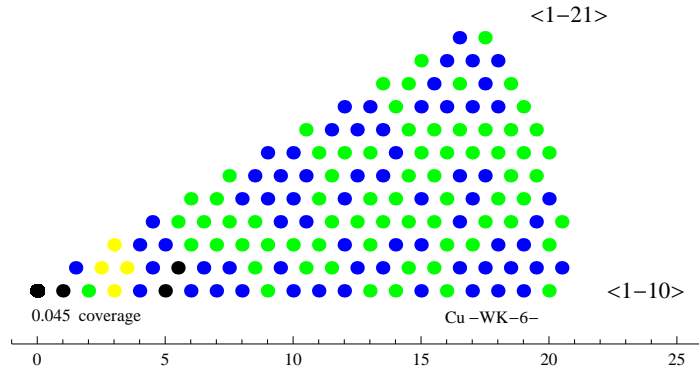


Fig.5.j shows an average pair distribution with short range interaction $U_3(s, \phi)$ (2.3) at coverage $\theta=0.045$.

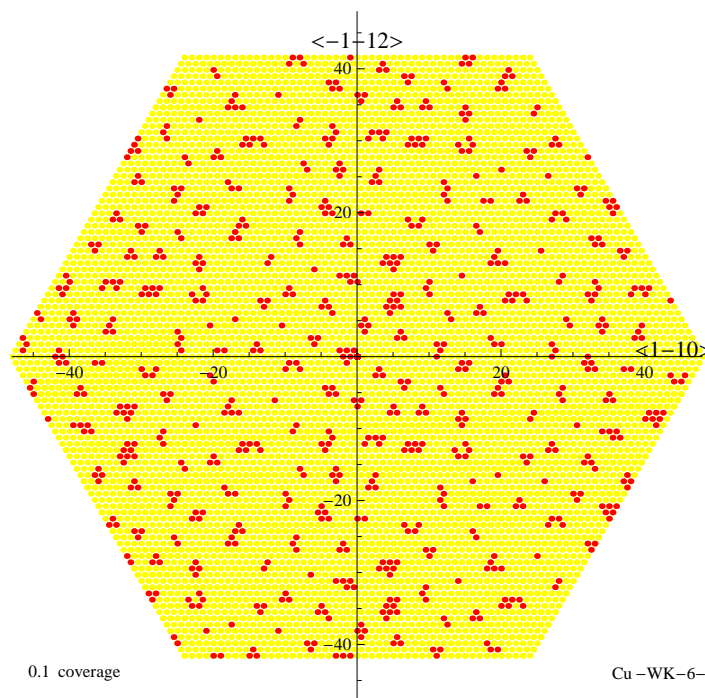


Fig.5.k shows a sample configuration with short range interaction $U_3(s, \phi)$ (2.3) at coverage $\theta=0.1$.

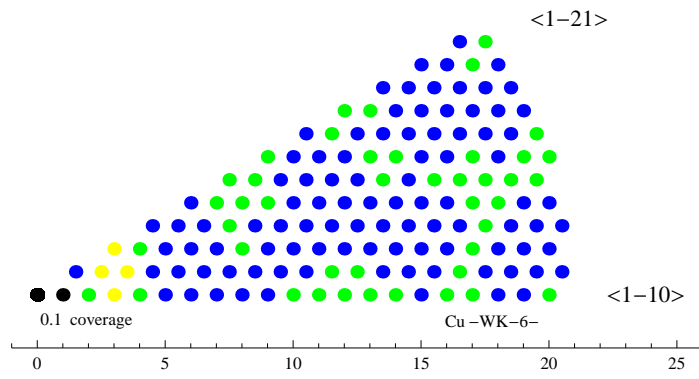


Fig.5.1 shows an average pair distribution with short range interaction $U_3(s, \phi)$ (2.3) at coverage $\theta=0.1$.

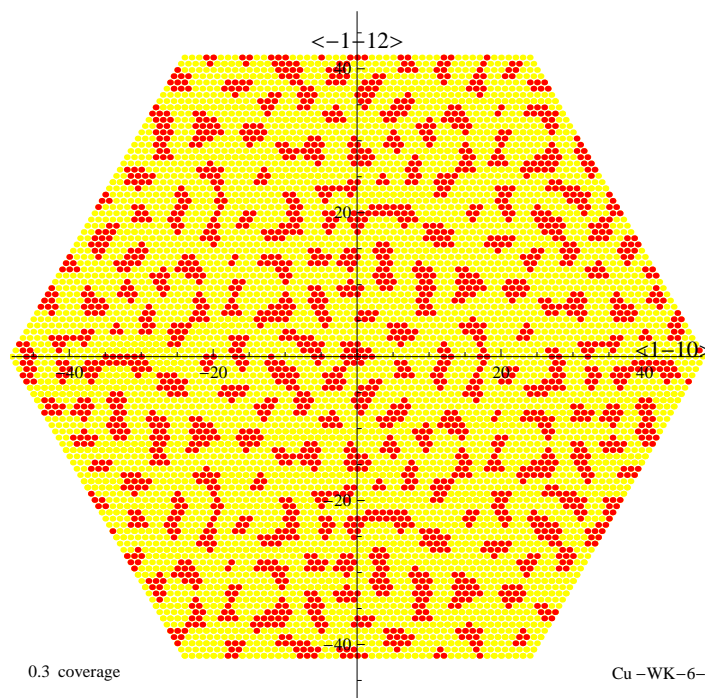


Fig.5.m shows a sample configuration with short range interaction $U_3(s, \phi)$ (2.3) at coverage $\theta=0.3$.

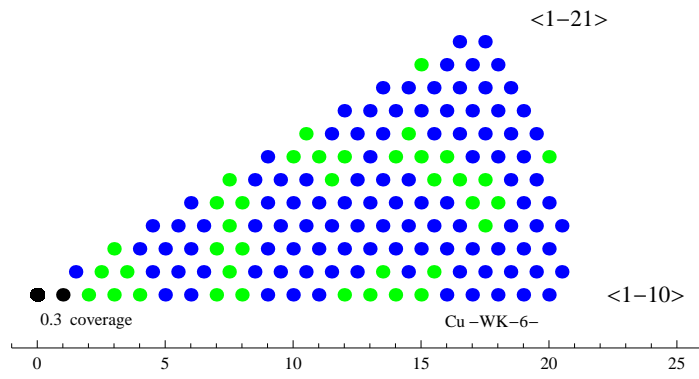


Fig.5.n shows an average pair distribution with short range interaction $U_3(s, \phi)$ (2.3) at coverage $\theta=0.3$.

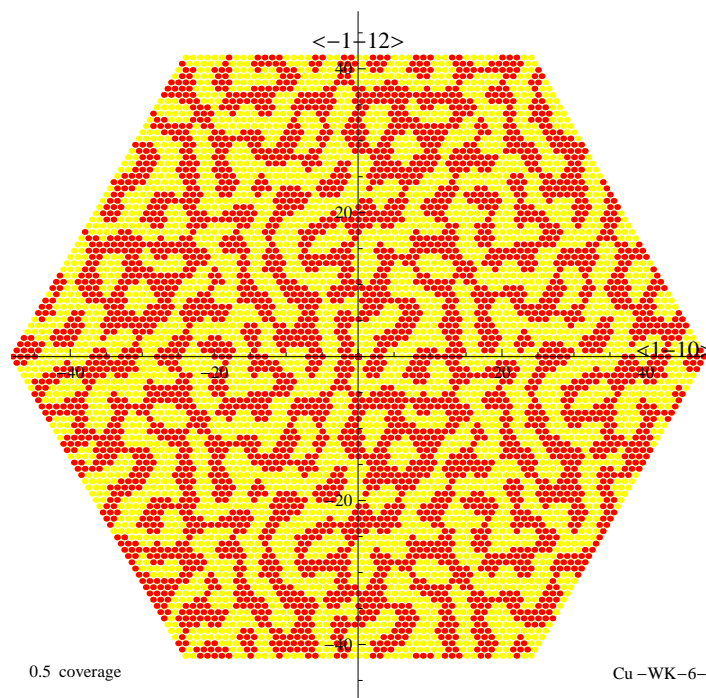


Fig.5.o shows a sample configuration with short range interaction $U_3(s, \phi)$ (2.3) at coverage $\theta=0.5$.

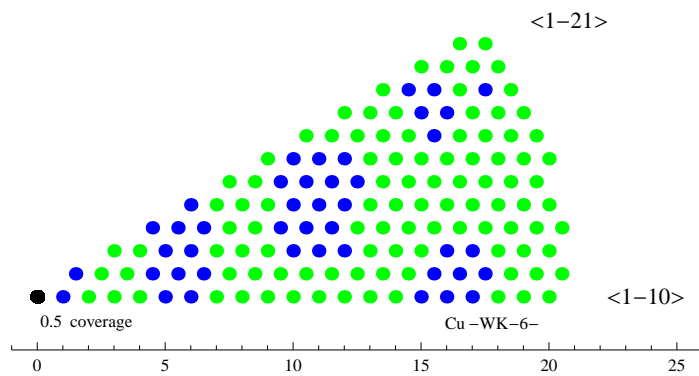


Fig.5.p shows an average pair distribution with short range interaction $U_3(s, \phi)$ (2.3) at coverage $\theta=0.5$.
 © Wolfgang Kappus 2012